Anal. Bioanal. Electrochem., Vol. 17, No. 4, 2025, 311-326
https://www.doi.org/10.22034/abec.2025.723273

Analytical & Bioanalytical Electrochemistry

Full Paper

Bifunctional Hydrogen and Oxygen Electrocatalysis of Cerium Doped Copper Oxide Nanostructure

Sabina Dahal, Prabin Kumar Joshi, Namrata Shree Pandey, Soniya Gadal, and Dasu Ram Paudel*

Department of Chemistry, Tri-Chandra Multiple Campus, Tribhuvan University, Kathmandu 44613, Nepal

*Corresponding Author, Tel.: +977-9849888864
E-Mail: dasu.paudel@trc.tu.edu.np

Received: 14 February 2025 / Received in revised form: 14 April 2025 / Accepted: 25 April 2025 / Published online: 30 April 2025

Abstract- *Artemisia vulgaris* contains bioactive compounds that act as reducing and stabilizing agents during nanoparticle formation, affecting their size and morphology. This study focuses on the eco-friendly green synthesis of cerium-doped copper oxide (Ce-CuO) nanoparticles, which minimizes hazardous waste. The nanomaterials were characterized using X-ray diffraction (XRD), Field emission scanning electron microscopy (FE-SEM), and Fourier-transform infrared spectroscopy (FTIR). The crystalline size was 14.4 nm, with FTIR confirming successful cerium incorporation into the copper oxide matrix and the FE-SEM revealed rough porous surfaces. The electrochemical properties of pristine CuO and Ce-CuO were inspected using a three-electrode setup. The overpotentials for HER were 145 mV at 50 mA cm^{-2} and 158 mV at 100 mA cm^{-2}, while for OER, they were 370 mV and 330 mV, respectively, indicating a marked improvement over pure CuO. The charge transfer resistance (R_{ct}) values were 7.67 Ω for HER and 1.76 Ω for OER, both lower than those of pure CuO. Doping cerium (Ce) in copper oxide (CuO) enhances its catalytic properties, electronic characteristics, and sensitivity. This approach offers new opportunities for Ce-doped CuO nanoparticles in applications like fuel cells, catalytic processes, and green hydrogen production.

Keywords- Green synthesis; Electrochemical water splitting; Ce-doping; Hydrogen evolution reaction; Oxygen evolution reaction

1. INTRODUCTION

Nanomaterials are important for energy-related applications, including energy production and storage, energy saving, energy transmission, and conversion. Surface area, energy, and chemistry are crucial factors in energy application, including physical and chemical interactions at the interface [1,2]. Nanoparticles have an important role in future energy technologies, necessitating cost-effective ways of large-scale manufacture. Nano-structured materials are vivacious for generating energy vectors to replace fossil fuels through renewable energy sources [3]. Hydrogen production through water splitting is a promising option for producing sustainable alternative energy in the 21st century. Due to society's need for clean and sustainable energy, deriving hydrogen energy through electrochemical water splitting is seen as a key path for future energy development. The electrolysis of water at the electrode surface necessitates active catalysts to enhance energy efficiency and significant endeavors to create an effective catalyst for viable green hydrogen production are required [4,5].

To synthesize nanomaterials with desired shapes, sizes, and specific functionalities, two fundamental approaches have been commonly established, the top-down method and the bottom-up approach [6]. Green chemistry is the concept of the design of chemical products and processes to minimize or eradicate the formation and use of hazardous substances, and an applicable approach across all aspects of chemistry [7]. Utilizing the twelve principles of green chemistry in nanoparticle synthesis through a bottom-up approach is a relatively new and important issue concerning sustainability. The conventional methods for the production of nanostructured materials are expensive, toxic, and non-environmentally friendly. To address these issues, precise green routes have been developed, that is the naturally occurring materials and their products that can be used for the synthesis of nanostructured materials by utilizing microorganisms such as fungi, yeasts, or use of plants and plant extracts [8].

Transition metal oxides are cheaper and now widely available alternatives to expensive precious metals. They are being studied as catalysts because they can effectively speed up important chemical reactions and are more sustainable for large-scale use [9,10]. Moreover, the electrocatalytic applications of transition metal oxides are commended owing to their existence of partially filled d-orbital, possessing unique reactivity, conductivity, and flexibility on electronic modulation. The Copper oxide nanomaterials are good contenders among many TMOs making them an ideal water-splitting catalyst for producing green hydrogen readily due to their particular qualities, such as being naturally available, highly reactive, cost-effective, nontoxic, and reversible redox properties [11]. The electronic modulation by a cation doping in the host lattice of CuO causes the compressive strain within the crystal lattice which facilitates the adsorption of key intermediates during the water-splitting reaction [12]. Doping of cations having larger size like Ce (a rare earth element) on the CuO matrix alters the structural, electronic, surface, and valence state thus enabling the catalytic parameters due to the generation of hybrid active sites. Rodney studied the bifunctional water splitting activity of

lanthanum doped CuO ($Cu_{1-x}La_xO$) in 1M KOH and found strong OER activity with a reduced potential of 1.552 V vs RHE and HER performance with -0.173 V vs RHE at 10 mA cm^{-2} as well as a pronounced overall water-splitting potential of 1.6 V at 10 mA cm^{-2}. In the quest for clean energy in our modern industrial age, cerium-doped copper oxide emerges as a practical and sustainable electrocatalyst for hydrogen production through water splitting. It provides an eco-friendly and cost-effective alternative to pricey precious metals. [13] Electrochemical water splitting (EWS) is a highly promising green energy technology that produces net-zero emissions and portable hydrogen fuel. Additionally, it allows for efficient electrochemical energy conversion and large-scale hydrogen production [2,14]. It comprises two primary reactions: the oxygen evolution reaction (OER) at the anode and the hydrogen evolution reaction (HER) at the cathode. By facilitating the breakdown of water into hydrogen and oxygen gasses, these processes work together to provide a sustainable way to generate hydrogen [9,14].

Despite numerous studies on the green synthesis of copper oxide NPs using various plant extracts, there is only limited research, particularly on *Artemisia vulgaris* (Mugwort), and very little on the use of dopants such as Cerium in electrochemical applications. However, the precise role of *A. vulgaris* as a reducing and stabilizing agent in the synthesis of Ce-doped CuO NPs has not been investigated. It has been demonstrated in the literature that the alkaloid and steroid groups present in the leaf extract of *A. vulgaris* plant act as reducing and capping agents for the synthesis of NPs. The understanding of the combined advantages of Ce doping and plant-based synthesis could lead to the production of more efficient and environmentally friendly Ce-CuO nanomaterials. Addressing this gap could provide valuable insights for enhancing catalyst design and advancing green nanotechnology for potential applications in green energy harvesting through water splitting.

2. EXPERIMENTAL SECTION

2.1. Materials

Cupric Sulphate ($CuSO_4.5H_2O$) ≥ 98.5% from Thermo Fisher Scientific India Pvt. Ltd., Ammonium Cerium (IV) sulphate dihydrate [$(NH_4)_4Ce(SO_4)_4.2H_2O$] ≥ 98.0% from Merck Life Science Private Limited, India, Distilled water from Lifeline Drop Pvt. Ltd., Ethanol ≥ 99.9% from RCP distilleries India Pvt. Ltd. and NaOH ≥ 98% from Qualikems Lifesciences Pvt. Ltd. were used. The chemicals weren't refined before being used.

2.2. Collection and preparation of plant extract

The leaf extract of Mugwort (*Artemisia vulgaris)* was used as a reducing and stabilizing agent. Green and fresh leaves of *A. vulgaris* were collected from Mudkhu, Tarakeshwar Municipality, Kathmandu, Nepal, in the month of January. The collected leaves were cleaned

and washed 2-3 times by running tap water to remove any bio-contaminates, followed by distilled water.

The wet leaves were kept in the sun for a few hours to remove moisture present. Then the leaves were crushed into fine paste using mortar and pastel. In the beaker containing 200 ml of distilled water, about 30 gm of fine paste of leaves were kept. The mixture was then stirred using a magnetic stirrer at 70 ℃ for 1 hour The extract was allowed to cool and filtered using Whatman No. 40 filter paper. The extract was stored for further use.

2.3. Synthesis of CuO nanoparticles

In a beaker, 10 mmol of $CuSO_4.5H_2O$ (2.496 g) and 100 mL of distilled water were taken. The solution was stirred at 500 rpm for about 15 minutes, and 20 mL of plant extract was added slowly as a reducing and stabilizing agent. The mixture was allowed to stir using a magnetic stirrer. 2 mL of 10% NaOH solution was added dropwise to the mixture. The mixture was stirred constantly at 70 ℃and 600-650 rpm for 2 hours. The blue color of the mixture was changed to greenish-blue color which indicates the formation of NPs. Thus formed CuO NPs were separated by centrifugation. The obtained CuO NPs were oven-dried at 60 ℃. Finally, CuO NPs were collected after calcinated in a muffle furnace at 400 ℃ for 2 hours. The obtained CuO NPs were crushed into fine powder using mortar and pestle and stored for further characterization and applications.

2.4. Synthesis of Ce-dopped CuO NPs

Ce-doped CuO nanoparticle was synthesized by applying the same procedure as for pure CuO NPs by maintaining the molar ratio of the volume of precursor solution and plant extract. Higher doping levels can lead to lattice deformation, secondary phase development, and decreased conductivity, whereas lower doping levels may only slightly increase electrocatalytic activity since the dopants may not change the material's electrical characteristics, so 5% of Ce doped CuO NPs was prepared. For this, 2 mmol of $(NH_4)_4Ce(SO_4)_4.2H_2O$ (1.265 g) and 8 mmol $CuSO_4.5H_2O$ (1.997 g) were mixed in 100 mL DI water in a beaker, stirred using a magnetic stirrer until the homogeneous solution prepared. 20 mL of plant extract followed by 2 mL of 10% NaOH was added under gentle stirring at 70 ℃ for 2 hours. The nanoparticle formation was marked by a sharp colour change of the solution and the formation of colloidal mass. As the reaction proceeded, the mixture’s initial blue color changed into a greenish-blue shade and formation of precipitates began. Thus, formed NPs was allowed to cool. After that, the mixture was centrifuged at about 6500 rpm for about 10 minutes which was then washed with ethanol once, followed by water for 2-3 times to remove any impurities present. The product was then dried in an oven at 60 ℃ overnight. The dried sample was calcinated at 400 ℃ for 2 h in a muffle furnace to remove any organic residues.

2.5. Electrode preparation

The catalyst ink was made by utilizing the polymer blinder technique. The CuO and Ce-CuO NPs were weighed (5 mg each) separately and sonicated in a solution of 350 µL DI water, 50 µL polyvinyl alcohol, and 10 µL Nafion for 30 min. A cleaned 1 cm^2 bare Ni foam was coated with catalyst ink by drop casting the catalyst ink followed by oven drying in a vacuum, which is used as a working electrode for HER and OER activity [14]. Ni foam is preferred due to its large surface area, strong mechanical integrity superior conductivity, mechanical and chemical resilience. Its three-dimensional porous structure improves catalyst loading and electron transfer, making it suitable for HER and OER[15].

2.6. Physicochemical characterization

X-ray diffraction (XRD) patterns were obtained using X-ray diffractor (Model: Rigaku Corp. Model TTRX3) to determine the crystalline structure and size of Ce-doped CuO NPs. Fourier Transform Infrared Spectroscopic (FTIR, Model: PerkinElmer Spectrum IR Version 10.6.2) was used to determine the functional groups present on the formed NPs. Field Emission Scanning Electron Microscopy (FE-SEM Model JEO1-JSM-6701F: JEOL, Ltd., Japan) was used for morphology and the surface texture of the electrocatalyst nanomaterial.

2.7. Electrochemical characterization

On the CHI 660 electrochemical workstation, electrochemical characterization was performed. Samples were characterized using 1 cm^2 catalyst loaded Nickel foam (NF) in a three-electrode technique. A saturated Ag/AgCl electrode served as the reference electrode, while a graphite rod served as the counter electrode. 1M KOH that was N_2-saturated served as the electrolyte [14]. Hydrogen Evolution Reaction (HER) and Oxygen Evolution Reaction (OER) were measured using linear sweep voltammetry (LSV), electrochemical impedance spectroscopy (EIS), Tafel slope, etc.

3. RESULTS AND DISCUSSION

The Ce-doped copper oxide nanoparticles were prepared using the green synthesis method. The precursor salts were first combined in the appropriate proportions with NaOH and plant extract and agitated for two hours. Ce-doped CuO NPs outperformed pure CuO in terms of catalytic activity and stability. The doping of Ce into CuO nanoparticles enhances the electrocatalytic performance of the material by reducing the overpotential, facilitating charge transfer, and improving the morphology.

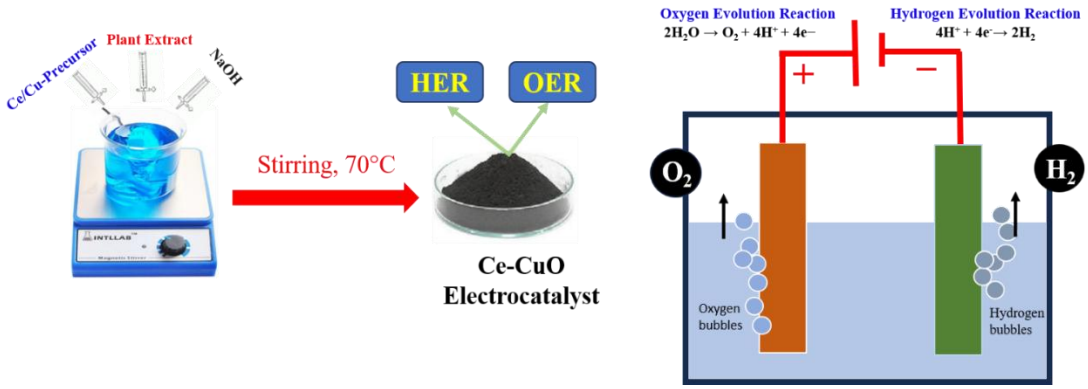

Scheme 1. Schematic diagram showing the synthesis and application of Ce-CuO NPs

3.1. Structural and morphological characterization

3.1.1. X-ray Diffraction (XRD)

The structural characteristics of the produced nanoparticles were determined using the XRD method. Figure 1 displays the XRD pattern of Ce-doped CuO NPs and CuO along with the stick pattern of matched JCPDs. The Ce-CuO NPs exhibits major diffraction peaks located at 35.52° and 39.12° corresponding to the crystal planes (002) and (200). The minor peaks are seen at 51.38° (112), 72.35° (311), and 83.06° (222). The major peaks of CuO NPs are also seen at 35.45° (002) and 38.92° (200). The minor peaks are seen at 51.34°,72.41°, and 83.42° corresponding to the planes (112), (311), and (222) respectively. They match with JCPDS 00-005-0661 [16].

The distinct and sharp peak indicates the successful synthesis of CuO and Ce-CuO signifying high crystallinity and purity [17]. The diffraction peak positions of CuO and Ce-CuO NPs are similar, with just a minor shift, indicating that the crystal structure is essentially unchanged. This suggests that the host lattice is not considerably disrupted by the relatively small dopant concentration. The average grain size of Ce-CuO NPs and CuO NPs was calculated by using Debye-Scherrer's equation (equation 1) with the help of High Score plus software which was found to be 14.4 and 14.44 nm respectively.

$$D = \frac{k\lambda}{\beta\cos\theta} \qquad (1)$$

Where,

D = crystalline size

K = Scherrer Constant

λ = X-Ray wave length

β = Full Width Half Maxima (FWHM)

θ = Bragg angle

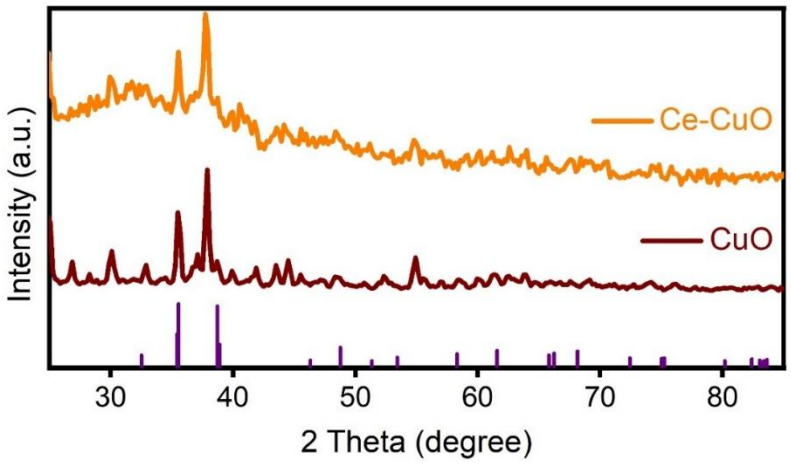

Figure 1. XRD pattern of CuO and Ce-doped CuO nanoparticles

3.1.2. Fourier Transform Infrared Spectroscopy

The spectra of pure CuO and Ce-doped CuO NPs is shown in Figure 2. The stretching bands at 2975 cm^{-1} and 1380 cm^{-1} are the result of C-H stretching vibration [18]. For pure and Ce-doped CuO, the band at around 483 cm^{-1} and 520 cm^{-1} corresponds to the characteristics of stretching vibration of M-O (Cu-O) bond [15]. The bond peak at 569 cm^{-1} is due to CuO stretching vibration [19]. In Ce-doped CuO, absorption peak are located at 1127 cm^{-1} is due to Ce-O-Ce bond [20] and 653 cm^{-1} is due to Ce-O [21] which confirms the doping of Ce in CuO nanoparticles.

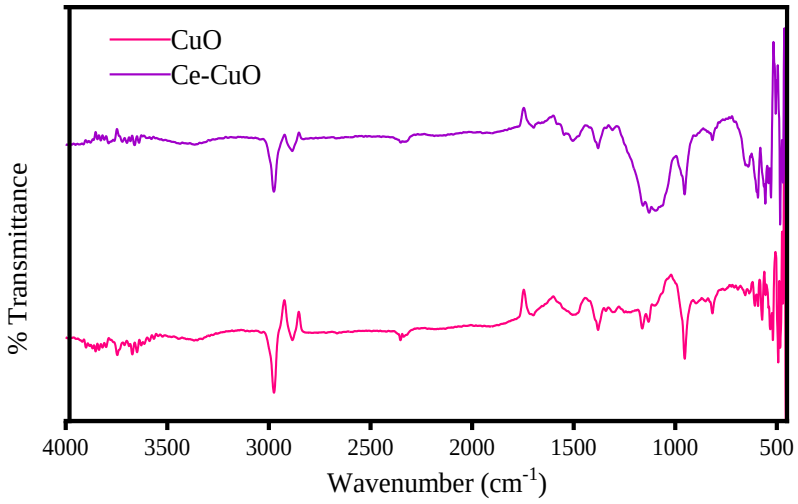

Figure 2. FTIR analysis of CuO and Ce-doped CuO nanoparticles

3.1.3 Field Emission Scanning Electron Microscopy (FESEM)

Figure 3 (a, b, and c) shows the FE-SEM images of Ce-doped CuO NPs at 1µm, 300 nm, and 100 nm range, respectively. The FE-SEM images display nanoparticles in the nanometer

range. The surface appears rough due to the presence of various aggregates or clusters. The increase in surface roughness and the more detailed appearance of the particles at higher magnification indicate that the particles provide large surface areas that are advantageous in various electrochemical applications.

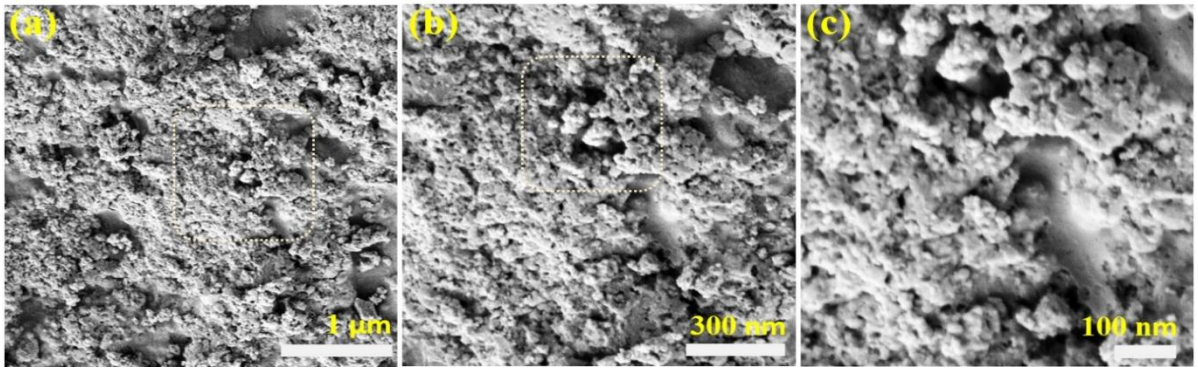

Figure 3. (a-c) FESEM images of the Ce-doped CuO NPs from lower to higher magnification (The box inside the image represents the magnification region)

3.2. Electrochemical Characterization

The hydrogen evolution reaction (HER) and the oxygen evolution reaction (OER) were thoroughly examined to evaluate the bifunctional capabilities of the catalyst that was synthesized. This investigation aimed to determine the effectiveness of the catalyst in facilitating both reactions, which are crucial for various energy conversion processes.

3.2.1. Hydrogen Evolution Reaction (HER)

In this study, we utilized a three-electrode system filled with nitrogen-saturated 1M KOH as the electrolyte to investigate the HER activity. We conducted linear sweep voltammetry (LSV) to assess the current response as a function of applied voltage, which provided insights into the reaction kinetics. Additionally, we examined the Tafel slope to evaluate the kinetic parameters and analyze the overpotential requirements for HER. To further understand the electrochemical characteristics of the system, we employed electrochemical impedance spectroscopy (EIS), which enabled us to study the charge transfer resistance and analyze the reaction mechanisms in detail.

3.2.1.1. Linear Sweep Voltammetry (LSV)

One electrochemical method for analyzing the redox behaviors of chemical species is linear sweep voltammetry which entails a single linear sweep from the lower to upper potential limit [22]. The efficacy of HER is based on the overpotential required to attain the benchmark current density of 50 mA cm^{-2} and 100 mA cm^{-2}. Figure 4 (a) displays, at a scan rate of 5 mV s^{-1}, the iR- corrected linear sweep voltammetry (LSV) data for HER of various samples. 95% iR

correction is performed to compensate for the voltage drop due to solution resistance. The iR-correction for HER and OER is calculated by using equation 2.

$$E_{corrected} = E_{RHE} - iR_s \quad (2)$$

Where, i = current passed, R_s = Solution resistance

Additionally, a scan rate of 5 mV s^{-1} was used to achieve a balance between experimental duration and diffusion-controlled behavior, thereby avoiding long measurement times that could lead to material degradation. This is because considerably lower scan rates (1–2 mV s^{-1}) may result in prolonged measurement times. It could result in ambient noise interference or even catalyst deterioration. This scan rate has been utilized in previous studies to achieve consistent and reproducible electrochemical assessments. Figure 4 (b) shows the plot of overpotential. A more efficient catalyst is indicated by a smaller overpotential seen in LSV. The electrochemical analysis of Ce-doped CuO indicated enhanced HER activity with a reduced overpotential value of 145 mV to reach a current density of 50 mA cm^{-2} and 158 mV for reaching 100 mA cm^{-2} current density. In contrast, pure CuO needed 198 mV and 219 mV overpotential for 50 mA cm^{-2} and 100 mA $cm^{-2,}$ respectively. The results demonstrate that the doping of Ce in CuO enhances the catalytic effectiveness due to intrinsic defects enriching catalytic active sites [23].

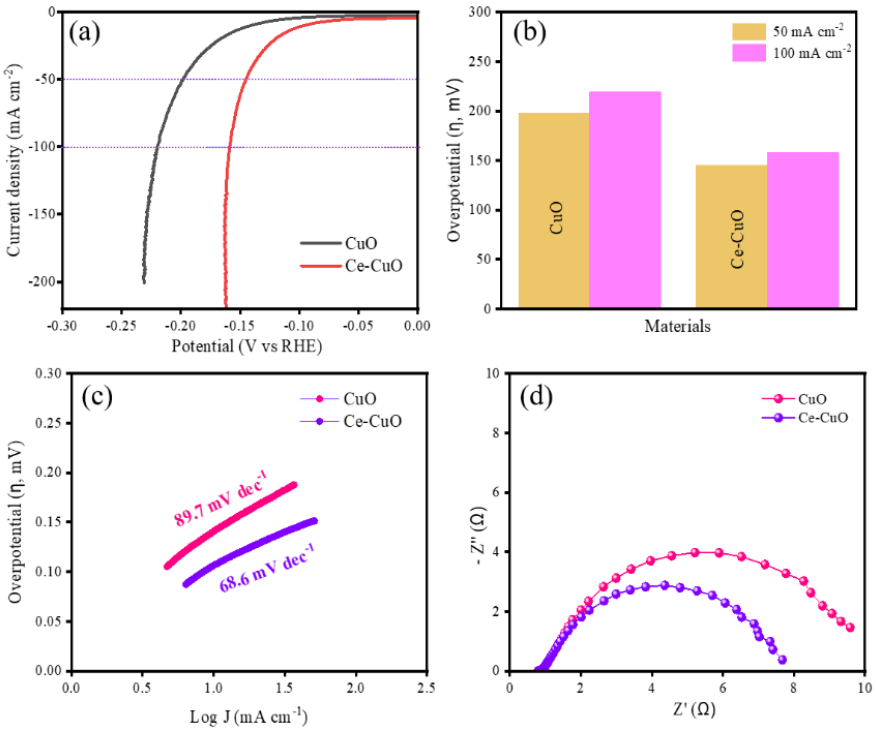

Figure 4. (a) Linear Sweep Voltammetry (LSV) measurement plots for the HER for individual catalysts; (b) Over potential plots for the HER of individual catalysts at different current densities; (c)Tafel plots of the individual catalysts; (d) Nyquist plot for individual catalyst

3.2.1.2. Tafel slope

Tafel slope had been used to evaluate the electrocatalyst's kinetic information. Tafel plot displays the dependency of steady-state current densities on various overpotential values. The overpotential (Z) has a logarithmic relationship with the current density (j), and the Tafel plot's linear component fits the equation ($\eta = a + b\log j$; where b = Tafel slope) [24]. The Tafel plot is obtained by replotting the polarization curves, which is the linear sweep voltammogram (LSV), as log current density (j) against overpotential. Figure 4 (c) shows the Tafel slope of pure CuO and Ce-doped CuO. Tafel slope for pure CuO and Ce-doped CuO was 89.7 mV dec^{-1} and 68.6 mV dec^{-1} which are comparable with LSV results. Ce-doped CuO has a lower Tafel slope than pure CuO. Lowering the Tafel slope implies increased catalytic activity making the reaction more efficient and faster [25]. Moreover, the Tafel slope values indicated that the rate-determining step follows the Volmer-Heyrovsky reaction kinetics, a most promising reaction mechanism for HER, involving adsorption of hydrogen on the catalyst surface and rapid desorption of H_2 molecule [26,27].

3.2.1.3. Electrochemical Impedance Spectroscopy (EIS)

EIS is a crucial electrochemical parameter to evaluate the interfacial properties of electrodes and chemical processes. Figure 4 (d) shows the Nyquist plots of pure CuO and Ce-CuO. The solution resistance (R_s) for pure CuO and Ce-CuO were found to be 0.891 Ω and 0.862 Ω respectively. Also, the charge transfer resistance (R_{ct}) was 9.57 Ω and 7.67 Ω for pure CuO and Ce-doped CuO respectively. The R_{ct} value is found to be lowered on a doping sample. Lower R_{ct} values of Ce-CuO suggest significantly increased electrocatalytic activity demonstrating improved charge transfer efficiency between electrode-electrolyte interfaces. Thus, the result disclosed a significant improvement in reversibility and conductance value when Ce is introduced into CuO lattice [28].

3.2.2. Oxygen Evolution Reaction (OER)

The performance of as synthesized electrode samples in the oxygen evolution reaction (OER) was thoroughly examined using a three-electrode setup with nitrogen-saturated 1M KOH as the electrolyte solution. We conducted OER analysis employing linear sweep voltammetry and electrochemical impedance spectroscopy to ensure the electrochemically sluggish reaction kinetics.

3.2.2.1. Linear Sweep Voltammetry (LSV)

Figure 5 (a) displays the iR-corrected linear sweep voltammetry (LSV) data, at a scan rate of 5 mV s^{-1}, for the OER of various samples. The OER overpotentials were determined using; $H_{OER} = E_{RHE} - 1.23V$. Figure 5 (b) shows the plot of overpotential. The electrochemical analysis of CuO and Ce-doped CuO indicated overpotential values of 310 mV and 270 mV respectively, to reach a current density of 50 mA cm^{-2}. For reaching 100 mA cm^{-2} current density, CuO has

an overpotential of 370 mV and Ce-CuO has an overpotential of 330 mV, which evidently indicates the low overpotential on doping of cation on CuO. Lower overpotential indicated higher catalytic efficiency. The results indicate that incorporating cerium (Ce) into copper oxide (CuO) nanoparticles (NPs) significantly increases their catalytic efficiency, presenting a promising approach to improve performance in electrochemical energy harvesting applications [24].

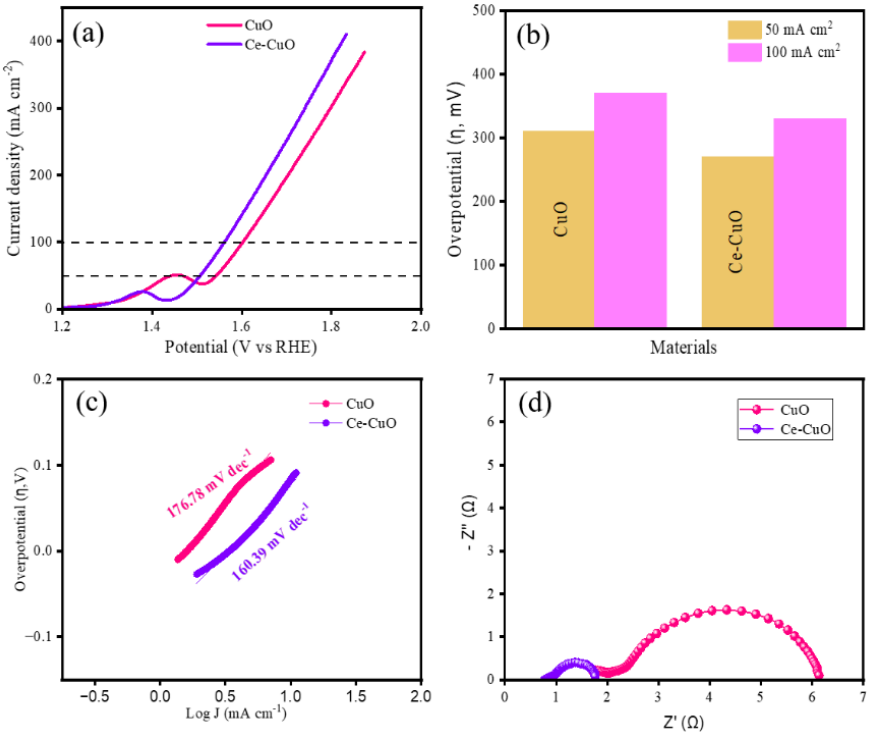

Figure 5. (a) LSV measurement plots for the OER of as-prepared catalysts; (b) Over potential plots for the OER of individual catalysts at 50 and 100 mA cm^{-2} current densities; (c) Tafel plots and Tafel slopes of the individual catalysts; (d) Nyquist plot for individual catalyst

3.2.2.2. Tafel slope

Figure 5 (c) demonstrates the Tafel slope of both CuO and Ce-doped CuO NPs. Tafel slopes for Pure CuO NPs is at 176.78 mV dec^{-1}. On the contrary, it drops to 160.39 mV dec^{-1} on the doping of Ce on CuO NPs. A drop in the Tafel slope of Ce-CuO signifies higher kinetic efficiency for electrochemical OER activity [26].

3.2.2.3. Electrochemical Impedance spectroscopy (EIS)

Figure 5 (d) shows the resulting Nyquist plots for pure CuO and Ce-CuO. Pure CuO has R_s and R_{ct} values of 1.71 Ω and 6.10 Ω, respectively. The R_s and R_{ct} values of Ce-CuO are 0.75 Ω and 1.76 Ω, respectively. The doping of Ce in CuO enhanced charge transfer compared to pure CuO. Lower values of R_s and R_{ct} both for Ce-CuO electrode suggest a much greater

electrocatalytic activity which can facilitate electron transfer more efficiently, leading to improved performance in electrochemical reactions [28].

3.2.2.4. Cyclic Voltammetry and Electrochemical Double-Layer Capacitor (EDLC)

Cyclic voltammetry is an essential and powerful technique for analyzing the redox properties of a wide range of chemicals. The intrinsic catalytic properties of the electrode material can be well evaluated by its surface area, the electrochemically active surface area (ECSA). We measure the double-layer capacitance (C_{dl}) of the as-synthesized electrode via the CV measurement within the non-Faradaic region at different scan rates, ranging from 50 mV s^{-1} to 100 mV s^{-1} (Figure 6a,b) [29,30]. The calculated slope of the electrode represents the C_{dl} and the following equation 3 is used to calculate electrochemically active surface area (ECSA),

$$ECSA = C_{dl}/C_s \quad (3)$$

where, C_s is the specific capacitance, C_{dl} is the electro-chemical double-layer capacitance[31].

The C_{dl} value of CuO is 6.71 mF cm^{-2} and that for Ce-CuO is 6.71 mF cm^{-2}, clearly suggesting a higher ECSA value [32]. Thus, the higher electrocatalytic performance of the Ce-doped CuO than that of pristine CuO is due to the increased surface area on doping of Ce on the CuO host i.e. higher electroactive surface area and increased exposed sites on the surfaces [33].

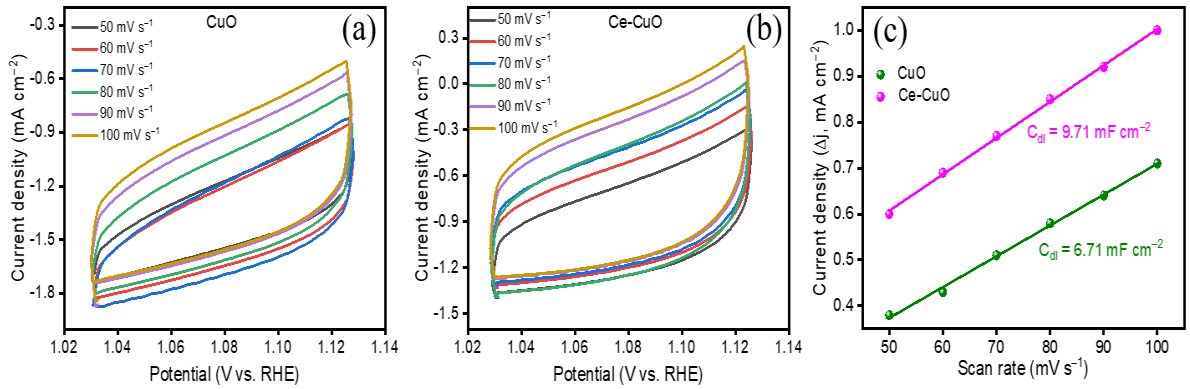

Figure 6. (a-b) CV measurement of CuO and Ce-CuO at different scan rates (c) Plot of scan rate versus current density (Δj) for the individual catalyst and their corresponding C_{dl} values

3.2.3. Chrono-potentiometric stability analysis

As an additional approach, the chrono-potentiometric method was used to investigate the electrocatalytic behavior of Ce-CuO nanoparticles as shown in Figure 7 (a and b). A steady current is passed between two electrodes, and the potential of one electrode is monitored over time with a reference electrode in this method [34]. To evaluate the hydrogen and oxygen evolution reactions, chronopotentiometry was performed by applying a constant current of 50 mA cm^{-2} for a period exceeding 24 hours. It was observed that there was no significant drop in

potential during the test for both HER and OER. This indicates excellent robustness of the electrode prepared with noteworthy electrochemical stability.

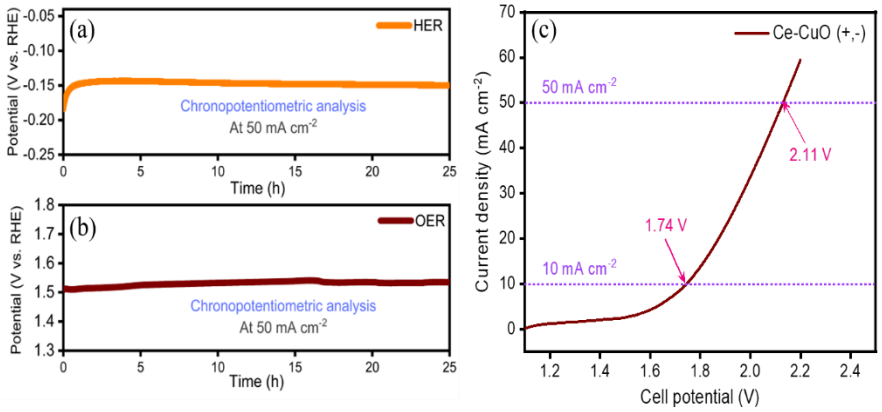

Figure 7. (a,b) Chrono-potentiometric long-term stability analysis of Ce-CuO for HER and OER respectively; (c) Polarization curve showing two-electrode system full-cell water splitting

3.2.4. Full-cell water splitting

The practical applicability of the electrodes as bifunctional electrocatalysts was then evaluated in a two-electrode full-cell water-splitting configuration. The polarization curve for the Ce-CuO system, used as both the cathode and anode, provides valuable insights into its performance. The Ce-CuO (+,-) system shows the cell potential of 1.74 V at 10 mA cm^{-2} and 2.11 V at 50 mA cm^{-2} (Figure 7c).

Table 1. Overpotential and Tafel slope values for the HER and OER of different catalysts

Sample	HER		OER		Ref.
	η_{HER}	Tafel Slope	η_{OER}	Tafel slope	
CuO	198 mV @ 50 mA cm^{-2}	89.7 mV dec^{-1}	310 mV@ 50 mA cm^{-2}	176.78 mV dec^{-1}	**Our work**
Ce-CuO	145 mV@ 50 mA cm^{-2}	68.6 mV dec^{-1}	270 mV@ 50 mA cm^{-2}	160.39 mV dec^{-1}	**Our work**
Co-CuO	-	-	299 mV@ 50 mA cm^{-2}	134 mV dec^{-1}	[36]
(Mo/Co)Ox–Cu@NF	188 mV@ 50 mA cm^{-2}	152 mV dec^{-1}	410 mV@ 50 mA cm^{-2}	276 mV dec^{-1}	[37]
CuO_x@Co_3O_4 NRs/CF	242 mV@ 50 mA cm^{-2}	61 mV dec^{-1}	240 mV@ 50 mA cm^{-2}	46 mV dec^{-1}	[38]
Cu_2S NRs@CoS/CF	324 mV@ 50 mA cm^{-2}	121 mV dec^{-1}	275 mV@ 50 mA cm^{-2}	54 mV dec^{-1}	[39]
CuO@CoS NRs	96 mV @10 mA cm^{-2}	-	246 mV@ 10 mA cm^{-2}	-	[40]
CuO@Cu_2O	135 @10 mA cm^{-2}	135mV dec^{-1}	315@10 mA cm^{-2}	63 mV dec^{-1}	[41]
CuO@Ni-P NA/CF	106@30 mA cm^{-2}	72mV dec^{-1}	275@30 mA cm^{-2}	124.9 mV dec^{-1}	[42]
CuO-NiO	38 @10 mA cm^{-2}	33mV dec^{-1}	172 @10 mA cm^{-2}	96 mV dec^{-1}	[43]
CuO@CoZn-LDH	124 @10 mA cm^{-2}	98.5mV dec^{-1}	194 @10 mA cm^{-2}	78.3 mV dec^{-1}	[44]
CuO/Co_3O_4	-	-	450 @50 mA cm^{-2}	42 mV dec^{-1}	[45]
CuO@Ni/NiFe	125 @10 mA cm^{-2}	86mV dec^{-1}	230 @10 mA cm^{-2}	65 mV dec^{-1}	[46]

This shows the relatively low cell voltage at different current densities which further indicates the suitability of the electrode in a bifunctional system for the generation of green hydrogen through a water-splitting process [35].

4. CONCLUSION

A safe environmentally friendly approach i.e. green synthesis was used to synthesize pure CuO, and Ce-doped CuO NPs. Adopting this method to synthesize NPs is quicker, cheaper, and more efficient as it doesn't result in the creation of any hazardous chemicals. It has been demonstrated that an extract from the leaves of *A. vulgaris* is an effective reductant for Copper NPs. X-ray diffraction (XRD), Field emission scanning electron (FE-SEM), and Fourier transfer infrared spectroscopy (FTIR) were used to analyze the structural and morphological characteristics of Ce-doped CuO NPs. The average size was 14.4 nm, according to XRD. From FTIR, Cu-O stretching band was revealed in pure CuO NPs and both Cu-O and Ce-O were seen in Ce-CuO NPs. Compared to pure CuO, Ce-doped CuO NPs exhibit enhanced catalytic activity and stability. The enhancement in electrochemical properties is due to the doping of Ce in CuO, which facilitates better electrolyte diffusion and lowers resistance, thereby improving electrochemical performance.

Acknowledgments

The authors feel grateful to Tri-Chandra Multiple Campus for facilitating the laboratory work, the FNCL lab at Jeonbuk National University, South Korea, for providing access to FE-SEM, LSV, and EIS characterization, Amrit Campus, Kathmandu for FTIR analysis, and NAST, Lalitpur for XRD analysis.

Declarations of interest

The authors declare the research work has no financial gain, personal benefit, or affiliations with any individual or organization and is free from extraneous influences that could compromise its integrity or objectivity.

REFERENCES

[1] Q. Zhang, E. Uchaker, S.L. Candelaria, and G. Cao, Soc. Rev. 42 (2013) 3127.

[2] C.C. Gudal, U.N. Pan, D.R. Paudel, M.R. Kandel, N.H. Kim, and J.H. Lee, ACS Appl. Mater. Interfaces 14 (2022) 14492.

[3] F. Raimondi, G.G. Scherer, R. Kötz, and A. Wokaun, Angew. Chemie - Int. Ed. 44 (2005) 2190.

[4] H. Li, Y. He, T. He, H. Shi, H. Yu, X. Ma, Y. Zhang, and C. Zhang, S. Wang, J. Solid State Chem. 289 (2020) 121498.

[5] Paudel, D. R., Kaphle G. C., Poudel, B. R., KC, M., Singh, M., and G.P. Ojha, Electrochem. 6 (2025) 3.
[6] N. Baig, I. Kammakakam, and W. Falath, I. Kammakakam, Mater. Adv. 2 (2021) 1821.
[7] P. Anastas, and N. Eghbali, Chem. Soc. Rev. 39 (2010) 301.
[8] M. Rafique, I. Sadaf, M.S. Rafique, and M.B. Tahir, Nanomedicine Biotechnol. 45 (2017) 1272.
[9] D.R. Paudel, U.N. Pan, R.B. Ghising, M.R. Kandel, S. Prabhakaran, D.H. Kim, and N.H. Kim, Appl. Catal. B Environ. 331 (2023) 122711.
[10] W. Xiong, H. Yin, and T. Wu, H. Li, Chem. A Eur. J. 29 (2022).
[11] M. Sajid, W. Qayyum, A. Farhan, M.A. Qamar, and H. Nawaz, Int. J. Hydrogen Energy 62 (2024) 209.
[12] X. Wu, Z. Tong, Y. Liu, Y. Li, Y. Cheng, J. Yu, P. Cao, C. Zhuang, Q. Shi, N. Liu, X. Liu, H. Liang, and H. Li, Nano Res. 17 (2024) 7194.
[13] J.D. Rodney, S. Deepapriya, M. Cyril Robinson, C. Justin Raj, S. Perumal, B.C. Kim, and S. Jerome Das, Int. J. Hydrogen Energy 45 (2020) 24684.
[14] D.R. Paudel, U.N. Pan, R.B. Ghising, P.P. Dhakal, V.A. Dinh, H. Wang, N.H. Kim, and J.H. Lee, Nano Energy 102 (2022) 107712.
[15] M.R. Islam, M. Saiduzzaman, S.S. Nishat, A. Kabir, and S.F.U. Farhad, Colloids Surfaces A Physicochem. Eng. Asp. 617 (2021) 126386.
[16] B.H.R. Suryanto, Y. Wang, R.K. Hocking, W. Adamson, and C. Zhao, Nat. Commun. 10 (2019) 1.
[17] S. G, R. S, P. E, H.A. Alhadlaq, R. Mohan, and A. G, M. Ahamed, J. King Saud Univ. Sci. 34 (2022) 102092.
[18] S. Jayakodi, and V.K. Shanmugam, Biointerface Res. Appl. Chem. 10 (2020) 6343.
[19] A. ur Rehman, M. Aadil, S. Zulfiqar, P.O. Agboola, I. Shakir, M.F. Aly Aboud, and S. Haider, Ceram. Int. 47 (2021) 5929.
[20] C.S. Transactions, and S. Parvathy, Chem. Sci. Trans. 6 (2017) 513.
[21] K. Hamidian, M.R. Saberian, A. Miri, F. Sharifi, and M. Sarani, Ceram. Int. 47 (2021) 13895.
[22] J.A. Rogers, A.A. Maznev, and M.J. Banet, K.A. Nelson, (2000).
[23] D.P. Jaihindh, P. Anand, R.-S. Chen, W.Y. Yu, M.S. Wong, Y.P. Fu, and J. Environ. Chem. Eng. 11 (2023) 109852.
[24] X. Zou, and Y. Zhang, Chem. Soc. Rev. 44 (2015) 5148.
[25] B.J. Kim, E. Fabbri, D.F. Abbott, X. Cheng, A.H. Clark, M. Nachtegaal, M. Borlaf, I.E. Castelli, T. Graule, and T.J. Schmidt, J. Am. Chem. Soc. 141 (2019) 5231.
[26] D.D. Qin, Y. Tang, G. Ma, L. Qin, C.L. Tao, and X. Zhang, Z. Tang, Int. J. Hydrogen Energy 46 (2021) 25771.
[27] D.R. Paudel, U.N. Pan, T.I. Singh, C.C. Gudal, N.H. Kim, and J.H. Lee, Appl. Catal. B

Environ. 286 (2021) 119897.
[28] A.S. Bhatt, R. Ranjitha, M.S. Santosh, C.R. Ravikumar, S.C. Prashantha, and R.R. Maphanga, Materials (Basel) 13 (2020) 1.
[29] R. Parsons, J. Electroanal. Chem. Interfacial Electrochem. 305 (1991) 164.
[30] F. Scholz, Electroanal. Methods Guid. to Exp. Appl. (2010) 1–359.
[31] E.S. Rountree, B.D. McCarthy, T.T. Eisenhart, and J.L. Dempsey, Inorg. Chem. 53 (2014) 9983.
[32] P. Sharma, and T.S. Bhatti, Energy Convers. Manag. 51 (2010) 2901.
[33] T. Brousse, D. Bélanger, K. Chiba, M. Egashira, F. Favier, J. Long, J.R. Miller, M. Morita, K. Naoi, P. Simon, and W. Sugimoto, Springer Berlin Heidelberg, Berlin, Heidelberg, (2017) 495.
[34] X. Xiong, C. You, Z. Liu, A.M. Asiri, and X. Sun, ACS Sustain. Chem. Eng. 6 (2018) 2883.
[35] Y. Ullal, and A.C. Hegde, Int. J. Hydrogen Energy 39 (2014) 10485.
[36] P. Babar, K. Patil, J. Mahmood, S. Kim, J.H. Kim, and C.T. Yavuz, Cell Reports Phys. Sci. 3 (2022) 100762.
[37] A.R. Tartour, M.M.S. Sanad, I.S. El-Hallag, and Y.I. Moharram, Sci. Rep. 14 (2024) 1.
[38] Q. Zhou, T.-T. Li, J. Qian, Y. Hu, F. Guo, and Y.Q. J. Mater. Chem. A 6 (2018) 14431.
[39] A.S. Sabir, E. Pervaiz, R. Khosa, and U. Sohail, RSC Adv. 13 (2023) 4963.
[40] J. Yang, H. Xuan, G. Zhang, R. Wang, J. Yang, X. Liang, and Y. Li, P. Han, Appl. Surf. Sci. (2021) 570.
[41] X.X. Ma, L. Chen, Z. Zhang, and J.L. Tang, 48 (2020) e20001.
[42] Chang, B., Hao, S., Z. Ye, and Yang, Y. (2018). 2393.
[43] Z. Guo, X. Wang, Y. Gao, and Z. Liu, Dalt. Trans. 49 (2020) 1776.
[44] L. Yin, X. Du, C. Di, M. Wang, K. Su, and Z. Li, Chem. Eng. J. 414 (2021).
[45] S.Y. Zhang, H.L. Zhu, and Y.Q. Zheng, Electrochim. Acta 299 (2019) 281.
[46] Y. Liu, Z. Jin, X. Tian, X. Li, Q. Zhao, and D. Xiao, Electrochim. Acta 318 (2019) 695.